Journal of Environmental Management 410 (2026) 130111

Contents lists available at ScienceDirect

Journal of Environmental Management

journal homepage: www.elsevier.com/locate/jenvman

Research article

Tracking the trajectory of mangrove dynamics in the Zambezi Delta, East Africa's largest river Delta

Tianliang Wu [a,1], Aoyang He [b,1], Zhijun Dai [b,c,*], Yan Li [a], Binyuan He [a], Qingxian Cao [a], Jinlan Lin [a], Xixing Liang [a,b,c]

[a] *Guangxi Academy of Oceanography, Nanning, 530022, China*
[b] *State Key Laboratory of Estuarine and Coastal Research, East China Normal University, Shanghai, 200062, China*
[c] *Guangxi Key Laboratory of Marine Environment Change and Disaster in the Beibu Gulf, Beibu Gulf University, Qinzhou, 535011, China*

ARTICLE INFO

Keywords:
Mangrove dynamics
Coastal erosion
Hydro-sediment dynamics
Tidal channels
Zambezi Delta

ABSTRACT

The Zambezi Delta hosts one of Africa's largest mangrove ecosystems, providing vital ecosystem services including carbon storage, coastal protection, and biodiversity support. However, the long-term spatiotemporal evolution of these mangroves and their responses to changing environmental drivers remain insufficiently understood. By integrating 35 years of Landsat imagery from 1989 to 2024 with fluvial sediment and hydrodynamic datasets, this study systematically investigates mangrove dynamics and their underlying mechanisms. The total mangrove area expanded at 307.08 ha yr^{-1} from 1989 to 2001, before declining at −107.47 ha yr^{-1} from 2001 to 2024. Spatially, the landward zone gained 2010 ha through encroachment into high-tide areas and tidal channels, whereas the mangrove seaward edge retreating at an average rate of −1.54 m yr^{-1}. Although fluvial sediment discharge increased, mangrove responses were highly non-linear and spatially heterogeneous, indicating that localized sediment redistribution was strongly modulated by hydrodynamic processes. Southeasterly waves promoted seaward edge retreat and sediment resuspension, while seasonal northeastward currents likely transported part of the resuspended sediment into tidal channels, where mangrove colonization and sediment trapping promoted channel narrowing. This expansion may have reduced upstream tidal connectivity, contributing to the replacement of upper-channel mangroves by terrestrial vegetation. Our findings reveal a coupled hydrodynamic and bio-geomorphic mechanism governing mangrove redistribution in the Zambezi Delta, with important implications for managing mixed-energy deltaic mangrove systems.

1. Introduction

Mangrove forests are critical intertidal ecosystems covering approximately 14.5 million ha globally, with ~40.5% situated along deltaic coasts (Jia et al., 2023; Worthington et al., 2020). Owing to their vast carbon storage capacity, with carbon stocks reaching up to 1023 t ha^{-1} (Donato et al., 2011), mangroves play an important role in climate-change mitigation (Murdiyarso et al., 2015). They bolster coastal resilience through wave energy attenuation; notably, a 100-m-wide mangrove belt can dissipate up to 66% of incoming wave forces, effectively safeguarding coastal communities, infrastructure, and seawalls (Menéndez et al., 2020; Zhou et al., 2022). Additionally, mangroves are fundamental to biodiversity conservation, water purification, and fisheries enhancement (Barbier et al., 2011; Hasim, 2021; Sasmito et al., 2023).

Despite their ecological and socioeconomic importance, global mangrove cover has declined substantially, losing approximately 524,500 to 677,000 ha over the past two decades (Bunting et al., 2022; FAO, 2023). However, this overall decline masks significant regional and local divergences; for instance, widespread losses in Southeast Asia and the Americas contrast with net expansions in countries like China and Australia (Bryan-Brown et al., 2020; Lymburner et al., 2020; Wang et al., 2022). This spatial heterogeneity is particularly pronounced in deltaic systems, where mangroves frequently exhibit simultaneous yet contrasting dynamics—such as landward retreat or encroachment, seaward expansion or erosion, and the colonization of tidal channels (Dai et al., 2024; Wu et al., 2025a; Xiong et al., 2024; Zhou et al., 2024). These complex dynamics are highly dependent on the localized

* Corresponding author. State Key Laboratory of Estuarine and Coastal Research, East China Normal University, Shanghai, China.
E-mail address: zjdai@sklec.ecnu.edu.cn (Z. Dai).
[1] The two authors contribute equally to this work.

https://doi.org/10.1016/j.jenvman.2026.130111
Received 5 January 2026; Received in revised form 16 May 2026; Accepted 29 May 2026
Available online 4 June 2026

interplay between geomorphic settings, sediment transportation, hydrodynamic forces, and anthropogenic impacts.

Previous studies have significantly advanced our understanding of mangrove dynamics in purely river-, wave-, or tide-dominated deltas (Besset et al., 2019; Long et al., 2025; Rogers and Goodbred Jr, 2014). For instance, widespread mangrove retreat in the Mekong, Indus, and Ganges Deltas is largely driven by diminished fluvial sediment loads, groundwater extraction, and coastal erosion (Besset et al., 2019; Bhargava et al., 2021; Zhou et al., 2024). Conversely, expansions observed in the Nanliu, Red, and Porong River Deltas are primarily facilitated by sediment accretion and tidal-flat progradation (Besselly et al., 2021; Long et al., 2021, 2022). However, these classifications often struggle to explain systems where tidal influence and wave action interact to reshape shorelines and redistribute sediment. In mixed-energy deltas, mangroves may expand along sheltered tidal channels where tidal penetration promotes sediment deposition, while simultaneously retreating along wave-exposed seaward edges where erosion exceeds seedling survival thresholds.

Characterized as a tide-dominated system subject to significant supplementary wave energy (Nienhuis et al., 2020), the Zambezi Delta exhibits extensive mangrove forests across varying geomorphic settings—from sheltered tidal channels to exposed coastal fronts. This setting allows for a comprehensive analysis of the concurrent drivers of mangrove migration. Therefore, this study aims to: (1) quantify the spatiotemporal evolution of mangrove forests in the Zambezi Delta; (2) characterize the spatial patterns of loss, gain, and migration across different geomorphic settings; and (3) diagnose the environmental and anthropogenic drivers of these changes. By unravelling mangrove responses in this representative mixed-energy system, this study contributes to a more general, predictive framework for understanding mangrove evolution in complex deltaic environments globally.

2. Materials and methods

2.1. Study area

The Zambezi River Basin, originating in the eastern highlands of Angola, is the largest river system on the eastern African coast, featuring a 2660 km main channel and a 1,380,000 km^2 catchment (Fig. 1A). The Zambezi Delta exhibits a tropical savanna climate (mean monthly temperatures: 27–37 °C; annual precipitation: ~1400 mm) and experiences semi-diurnal tides with a 4.1 m maximum range, which penetrate up to 80 km upstream during the dry season (Barbosa et al., 2001; Bento et al., 2007; Tweddle et al., 2015). Wave activity is dominated by local winds, with significant wave heights from the south/southeast frequently exceeding 1 m (Mikhailov et al., 2015).

The delta hosts all eight mangrove species reported in Mozambique: *Sonneratia alba*, *Avicennia marina*, *Rhizophora mucronata*, *Ceriops tagal*, *Bruguiera gymnorrhiza*, *Lumnitzera racemosa*, *Heritiera littoralis*, and *Xylocarpus granatum* (Stringer et al., 2015; Trettin et al., 2016). Extending approximately 180 km along the coastline and up to 50 km inland, these mangrove forests form one of the largest continuous stands in Africa (Barbosa et al., 2001). To evaluate spatial variations in morphodynamics, the study area is partitioned into three zones (Fig. 1B): the Southeastern Part (SEP), an active delta lobe characterized by complex channels and direct fluvial input; and the Northeastern (NEP) and Southern (SP) Parts, which are inactive flanking lobes influenced primarily by marine forces.

2.2. Materials

Landsat imagery (1989–2024) was processed via the Google Earth Engine (GEE). To analyze drivers of mangrove dynamics, supplementary datasets were employed. Sediment discharge data (1989–2020) were

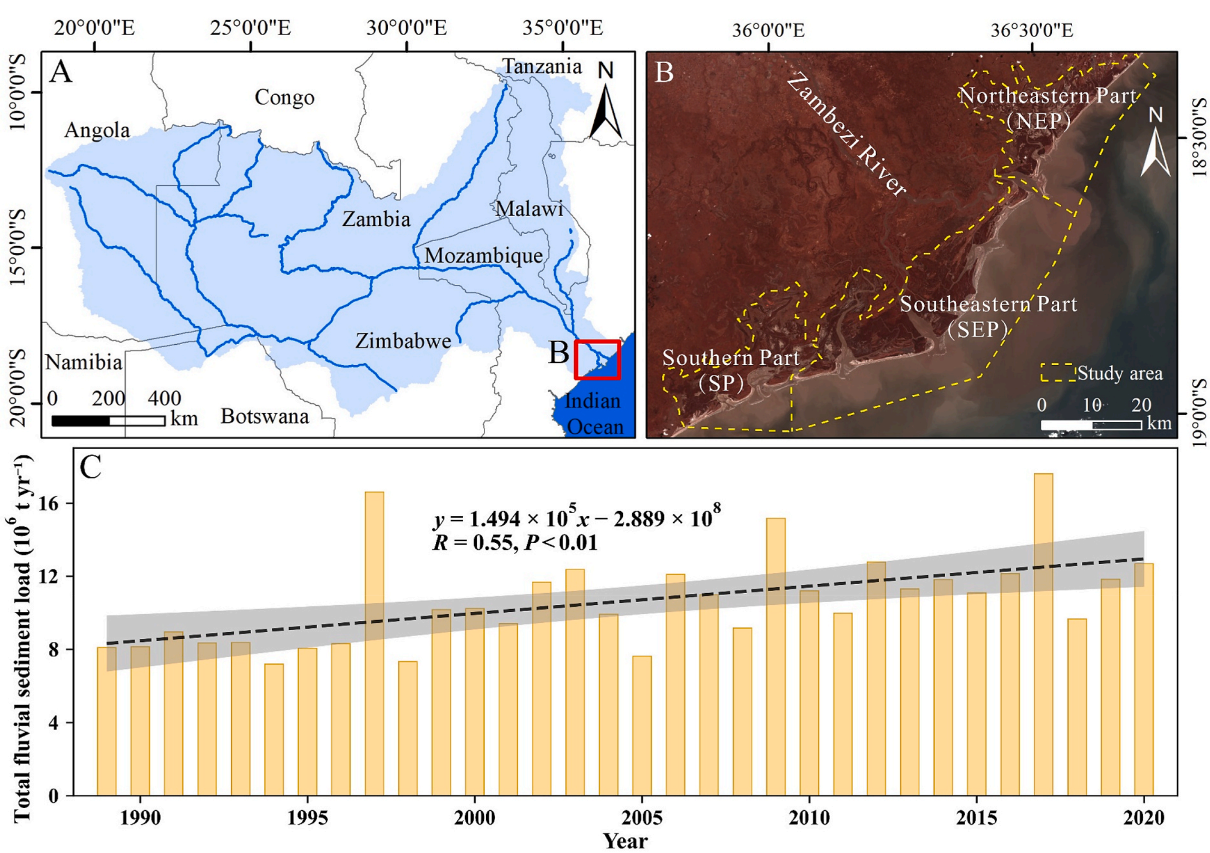

Fig. 1. (A) Location of the Zambezi River Basin and Delta. (B) Subdivision of the study area. (C) Time series and linear fitting trends of annual total fluvial sediment load between 1989 and 2020.

obtained from Dethier et al. (2022). Monthly ocean current data (1993–2024) from the Copernicus Marine Environment Monitoring Service (CMEMS) (Lellouche et al., 2021) provided eastward (u) and northward (v) velocity components for the study area (35.45°–36.755°E, 18.25°–19.25°S), processed in MATLAB to characterize seasonal ocean circulation. Hourly offshore wave records were extracted from the European Centre for Medium-Range Weather Forecasts (ECMWF) ERA5 dataset (Hersbach et al., 2023). Given the swell-dominated nature of the Mozambique Channel, wave energy predominantly originates from the SSW–SE sector (Mazzaretto and Menendez, 2024; Sreelakshmi and Bhaskaran, 2020). Frequency distributions for representative years (1989, 1996, 2003, 2010, 2017, and 2024) were analyzed to assess multi-decadal wave action. Wave direction and significant wave height were extracted for the NEP (36.5°E, 18.5°S), SEP (36.5°E, 19.0°S), and SP (36.0°E, 19.0°S). We applied a frequency distribution analysis, partitioning directions into 18 angular sectors (20°) and heights into discrete bins (0–1, 1–2, and 2–3 m) to identify dominant wave energy vectors via wave rose diagrams. Data and scripts are available via Mendeley Data (DOI: 10.17632/ywwkbz9pn7.1).

2.3. Methods

2.3.1. Land cover classification

We generated annual median composite land cover maps for the Zambezi Delta (1989–2024) using 829 Landsat TM, ETM+, and OLI scenes acquired from the GEE (Fig. S1; Table S1). All images underwent radiometric correction and pixel-based cloud/shadow masking. The annual median compositing approach was employed to minimize the effects of seasonal phenology and tidal fluctuations (Xiong et al., 2024).

Land cover classification was performed on the GEE utilizing a Random Forest classifier configured with 300 decision trees. The model utilized 13 input features—comprising six spectral bands and seven derived indices (Table 1)—to distinguish five land-cover classes: mangroves (intertidal woody plants), terrestrial vegetation (inland plants), bare tidal flats (unvegetated intertidal mud/sand), bare land (inland dry soils/impervious surfaces), and water. Spectrally, mangroves exhibit more pronounced shortwave infrared (SWIR) absorption than terrestrial vegetation due to periodic tidal inundation. Additionally, high moisture content causes bare tidal flats to display lower near-infrared (NIR) and SWIR reflectance compared to dry bare land, whereas water intensely absorbs both bands. Consequently, incorporating NDVI and EVI (for vegetation greenness), MVI and EMVI (to isolate mangroves), and NDWI, LSWI, and MNDWI (for water detection) substantially improved mapping accuracy.

Table 1
Spectral index for land cover classification.

Name	Formulas	References
Modified Normalized Difference Water Index (MNDWI)	$MNDWI = \frac{(\rho_{green} - \rho_{swir})}{(\rho_{green} + \rho_{swir})}$	Xu (2006)
Enhanced Vegetation Index (EVI)	$EVI = 2.5 \times \frac{(\rho_{swir} - \rho_{nir})}{(\rho_{nir} + 6\rho_{red} - 7.5\rho_{blue} + 1)}$	Huete et al. (2002)
Normalized Difference Vegetation Index (NDVI)	$NDVI = \frac{(\rho_{nir} - \rho_{red})}{(\rho_{nir} + \rho_{red})}$	Rouse et al. (1974)
Mangrove Vegetation Index (MVI)	$MVI = \frac{(\rho_{nir} - \rho_{green})}{(\rho_{swir} - \rho_{green})}$	Baloloy et al. (2020)
Enhanced Mangrove Vegetation Index (EMVI)	$EMVI = \frac{2\rho_{nir} - \rho_{green} - \rho_{swir}}{2\rho_{nir} + \rho_{green} + \rho_{swir})}$	Yang et al. (2022)
Normalized Difference Water Index (NDWI)	$NDWI = \frac{(\rho_{green} - \rho_{nir})}{(\rho_{green} + \rho_{nir})}$	McFeeters (1996)
Land Surface Water Index (LSWI)	$LSWI = \frac{(\rho_{nir} - \rho_{swir})}{(\rho_{nir} + \rho_{swir})}$	Gao (1996)

Note: ρ_{blue}, ρ_{green}, ρ_{red}, ρ_{nir}, and ρ_{swir} denote the blue, green, red, near infrared, and shortwave infrared bands of the Landsat imagery, respectively.

Training and testing datasets were generated via a stratified random sampling procedure. Ground-truth labels were primarily derived from the global mangrove database and visual interpretation of high-resolution Google Earth imagery (Table S1). For earlier epochs (e.g., 1989) lacking high-resolution data, samples were carefully identified using Landsat false-color composites based on established spectral and textural signatures. To mitigate spatial autocorrelation, samples were collected as isolated points rather than contiguous polygons or regions of interest (ROIs). During interpretation—particularly for early epochs reliant on Landsat imagery—we deliberately avoided selecting adjacent pixels within the same homogeneous patches, ensuring a broad distribution across diverse landscape contexts. Subsequently, a random number attribute was assigned to each sample, with 80% randomly allocated for training and the remaining 20% reserved for testing. We acknowledge that this random split does not equate to a fully spatially independent validation and cannot entirely eliminate spatial autocorrelation effects. Thus, the reported accuracy metrics represent an internal, point-based assessment rather than a strictly independent evaluation, a limitation particularly pertinent to early mapping years. Under this validation framework, overall accuracy and Kappa coefficients consistently exceeded 94% across all years (Fig. S1; Table S2–S5).

2.3.2. Trend and change analysis

Annual mangrove areas were quantified based on the classification results. To account for methodological uncertainties inherent in medium-resolution Landsat imagery (~0.09 ha/pixel)—including classification errors, mixed pixels, residual tides, and spatial autocorrelation—all total area estimates were conservatively rounded to the nearest 10 ha. Subsequently, the temporal dynamics of mangrove extent from 1989 to 2024 were evaluated through time-series trend analyses. Segmented linear regression was applied to objectively detect structural shifts in the time-series. Optimal breakpoints were determined using the Bayesian Information Criterion (BIC) and validated by permutation testing, confirming the segmented model significantly outperformed a global linear model ($P < 0.001$). Within each identified segment, ordinary least squares (OLS) regression was utilized to quantify the annual rate of change alongside its 95% confidence intervals and P-values.

To evaluate spatial dynamics while filtering out short-term interannual noise, the annual classification maps were aggregated into multi-year epochs (Xiong et al., 2024). Spatial overlay and land-cover transition analyses were conducted in ArcGIS to quantify patch-level gains, losses, and bidirectional conversions across five seven-year intervals (1989–1996 to 2017–2024) and the overarching study period. Land cover transitions focused on conversions between mangroves, terrestrial vegetation, bare land, and bare tidal flats (Wu et al., 2025b). Open water was excluded as a specific transition endpoint because regional mangroves are predominantly confined to intertidal flats near or above mean sea level. Consequently, seaward expansion generally follows tidal flat accretion, and seaward mortality typically presents as a conversion to bare tidal flats rather than directly to open water. Although abrupt erosion events may occasionally cause direct mangrove-to-water conversions, seaward edge dynamics were primarily interpreted through mangrove–tidal flat conversions.

Beyond the cross-class land cover conversions, we independently quantified specific mangrove area gains and losses over the identical temporal intervals to elucidate their cross-shore dynamics. Directional changes within each period were partitioned by designating the respective initial seaward mangrove edge as a baseline, thereby facilitating the discrete measurement of landward and seaward dynamics (Dai et al., 2024). Spatially, the landward zone was defined as the area extending from the initial seaward baseline toward the terrestrial interior, whereas the seaward zone comprised the prograding area extending toward the ocean—a domain directly governed by marine hydrodynamics.

2.3.3. Seaward edge analysis

By applying the previously defined seven-year intervals, the extraction of mangrove seaward edge dynamics mitigated the uncertainties associated with Landsat's 30 m spatial resolution and residual inter-annual tidal noise in the composite imagery. This ensures that genuine geomorphological migration signals surpass tidal-induced artifacts, a standard practice in mangrove change assessments (Xiong et al., 2024; Long et al., 2025). Rates of mangrove seaward edge migration across the discrete intervals and the overarching period were computed using the Digital Shoreline Analysis System (DSAS). The End Point Rate (EPR) was selected for its efficacy in period-to-period evaluations, yielding a robust annualized rate of change (Thieler et al., 2009). Spatially, 2113 shore-normal transects were cast at 50 m intervals across the Zambezi Delta (626 in the NEP, 1170 in the SEP, and 317 in the SP). The EPR was calculated as: $EPR = D_j - D_i / Y_j - Y_i$, where Y and D denote the year and the perpendicular distance from the baseline to the seaward edge at time steps j and i, respectively. Positive EPR values indicate seaward expansion, while negative values indicate landward retreat.

Pixel-scale classification uncertainties arise from a one-pixel positional error, which yields an approximate EPR uncertainty of ±4.3 m yr^{-1} over a 7-year interval. To account for this, a threshold-sensitivity analysis was conducted using ±0.5, ±1, ±2, and ±5 m yr^{-1}. Although the absolute proportions of retreating, stable, and expanding transects varied with threshold choice, the delta-wide Decrease/Increase ratio remained relatively stable across thresholds, ranging from 2.05 to 2.11 for thresholds of ±0.5 to ±2 m yr^{-1} and remaining above unity at 1.74 under ±5 m yr^{-1} (Table S6). Based on this sensitivity analysis and the Landsat pixel-scale uncertainty, a conservative ±5 m yr^{-1} threshold was adopted for final classification: transects with EPR < -5 m yr^{-1} were classified as retreating, those with EPR >5 m yr^{-1} as expanding, and those between −5 and 5 m yr^{-1} as stable.

3. Results

3.1. Temporal trends of mangrove extent

Over the 35-year period from 1989 to 2024, the mangrove extent of the Zambezi Delta exhibited two distinct phases of expansion and subsequent decline (Fig. 2A). Total mangrove area first expanded from 42,010 ha in 1989 to 45,680 ha in 2001 at a rate of 307.08 ha yr^{-1} (95% CI: 224.03–390.12; $P < 0.001$), and subsequently contracted to 43,080 ha by 2024 at −107.47 ha yr^{-1} (95% CI: −143.78 to −71.16; $P < 0.001$).

These delta-wide trends concealed pronounced sub-regional contrasts (Fig. 2B–D). The NEP sustained a continuous net gain composed of two phases: rapid expansion during 1989–1996 (361.99 ha yr^{-1}, 95% CI: 229.61–494.37; $P < 0.001$), followed by a slower but persistent increase through 2024 (26.63 ha yr^{-1}, 95% CI: 7.76–45.50; $P < 0.01$). The SEP exhibited a clear reversal, expanding from 23,980 ha in 1989 to 26,000 ha in 2008 (126.62 ha yr^{-1}, 95% CI: 75.31–177.94; $P < 0.001$) before declining to 23,610 ha by 2024 (−141.15 ha yr^{-1}, 95% CI: −177.51 to −104.79; $P < 0.001$). In contrast, the SP experienced a persistent net decline. Losses were modest before 1998 but accelerated thereafter, reaching −46.58 ha yr^{-1} between 1998 and 2024 (95% CI: −66.13 to −27.03; $P < 0.001$).

3.2. Spatial dynamics of mangrove forests

Mangrove gains in the Zambezi Delta declined progressively over time, from 6590 ha in 1989–1996 to 2480 ha in 2017–2024, with the reduction more pronounced on the landward than on the seaward side (Figs. 3 and 4A–B; Table S7 and S8). Mangrove losses, by contrast, showed no consistent temporal trend, averaging ~4560 ha per interval. As a result, the delta shifted from net gain (1890 ha in 1989–1996; 2570 ha in 1996–2003) to net loss in the three subsequent intervals (1050 ha, 690 ha, and 1650 ha, respectively), with both gains and losses dominated by landward dynamics (Figs. 3 and 4B; Table S7 and S8).

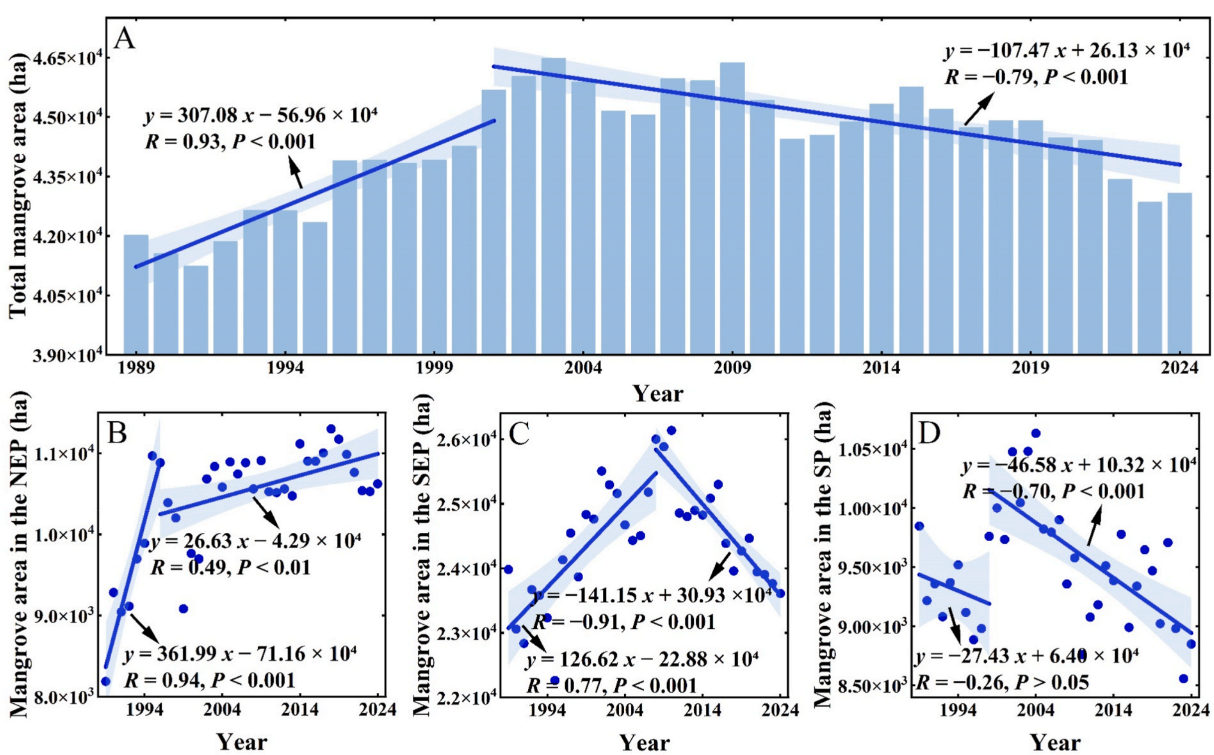

Fig. 2. Interannual trends of mangrove area in the Zambezi Delta (1989–2024). (A) Overall temporal trend across the entire delta. (B–D) Sub-regional trends for the NEP, SEP, and SP, respectively.

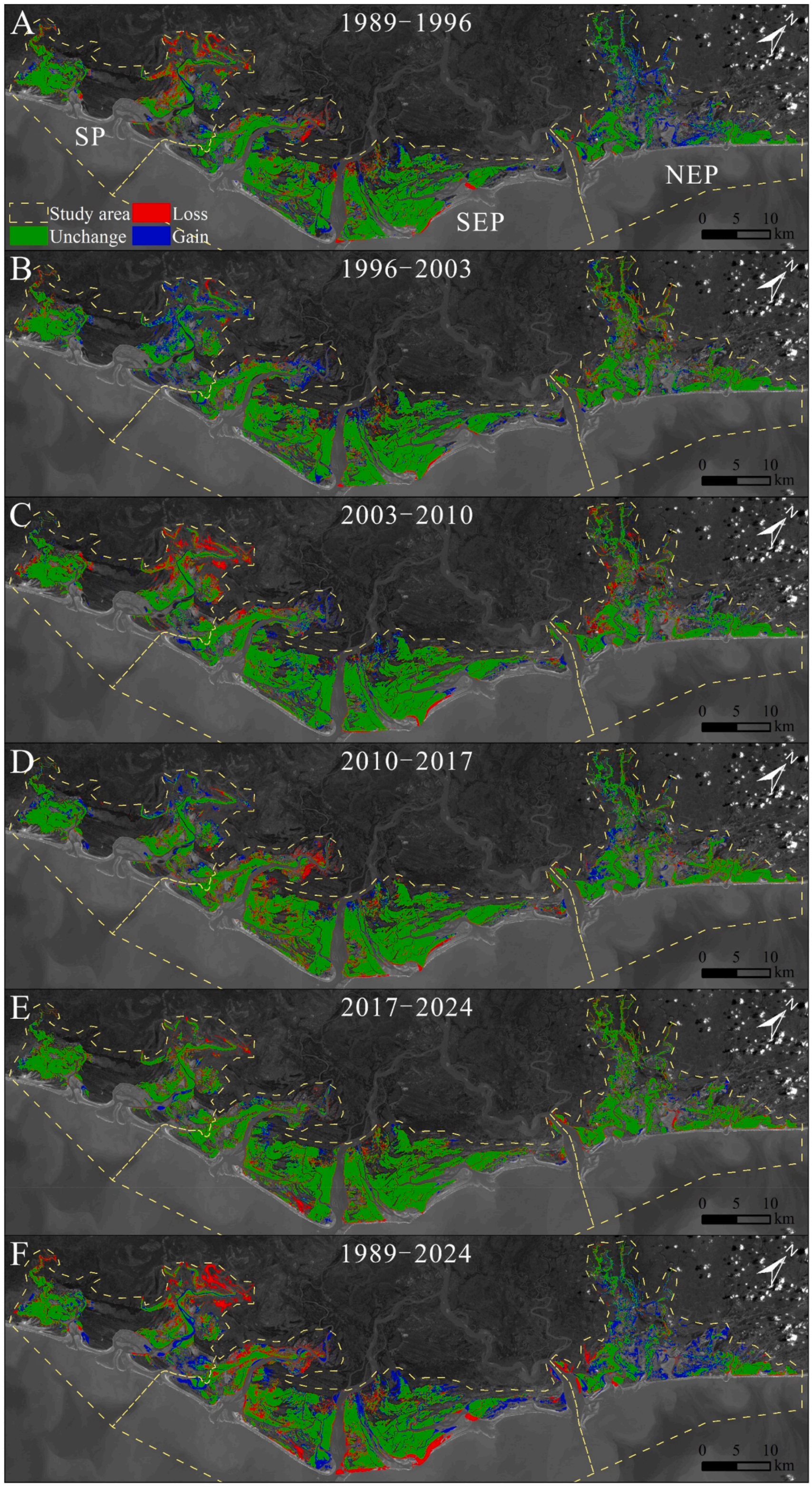

Fig. 3. Spatial dynamics of mangroves in the Zambezi Delta over (A–E) consecutive 7-year intervals and (F) the entire 1989–2024 period.

Cumulatively, mangroves displayed contrasting dynamics at their landward and seaward sides (Figs. 3 and 4D). The delta gained 2010 ha landward—2650 ha in the NEP and 400 ha in the SEP—while the SP lost 1040 ha. Landward gains in the NEP and SEP were concentrated along tidal channels and within the intertidal–terrestrial transition zone, whereas losses were focused on upstream flats (Fig. 3F). In the SP, dieback dominated upstream flats and was only partially offset by expansion onto downstream flats (Fig. 3F). Along the seaward edge, the delta lost 940 ha overall, primarily in the SEP (780 ha) and NEP (200 ha); the SP coastline showed a marginal seaward gain of 40 ha.

The seaward edge retreated overall, with a delta-wide mean EPR of -1.54 m yr^{-1} (Fig. 5). Applying the conservative ±5 m yr^{-1} threshold, 30.95% of transects were classified as retreating, 17.75% as expanding, and 51.30% as stable, yielding a Decrease/Increase ratio of 1.74

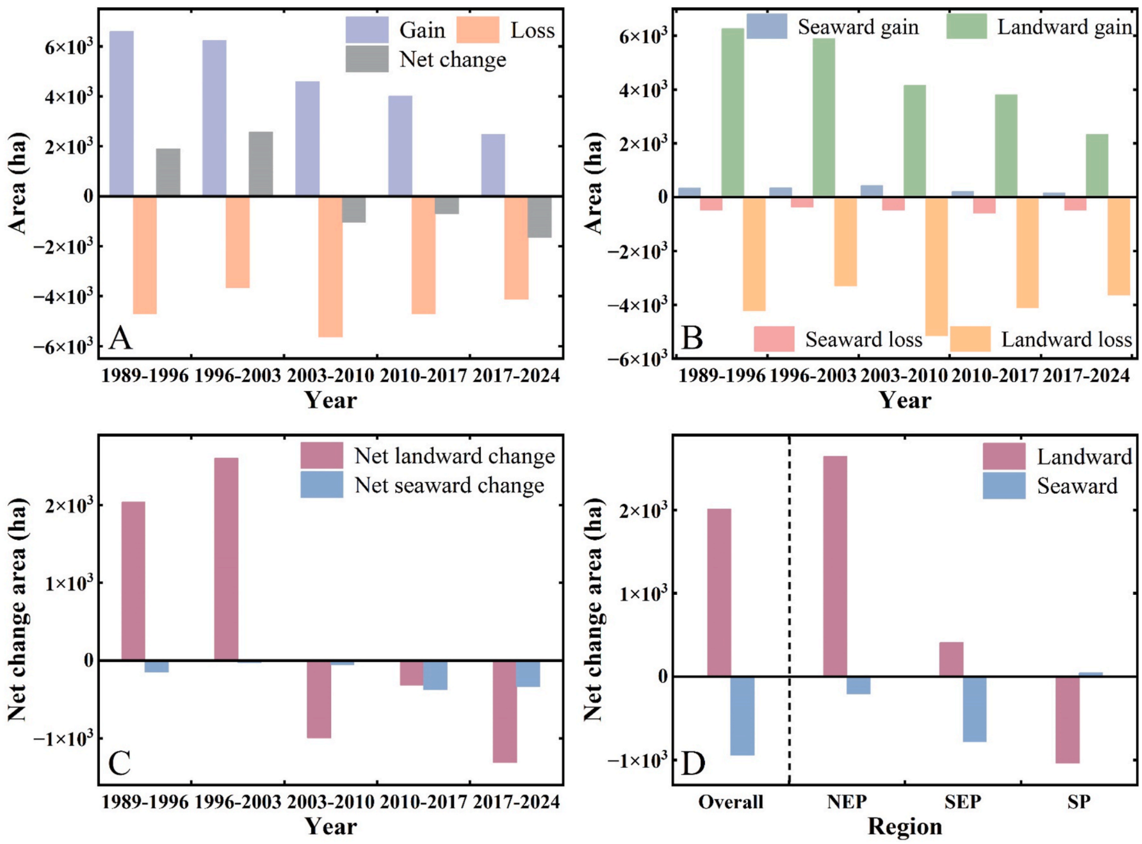

Fig. 4. Spatiotemporal dynamics of mangrove areas in the Zambezi Delta (1989–2024). (A) Overall area gains, losses, and net changes over time. (B) Specific landward and seaward gains and losses. (C) Net landward and seaward changes. (D) Net landward and seaward area changes for the overall Delta and its sub-regions.

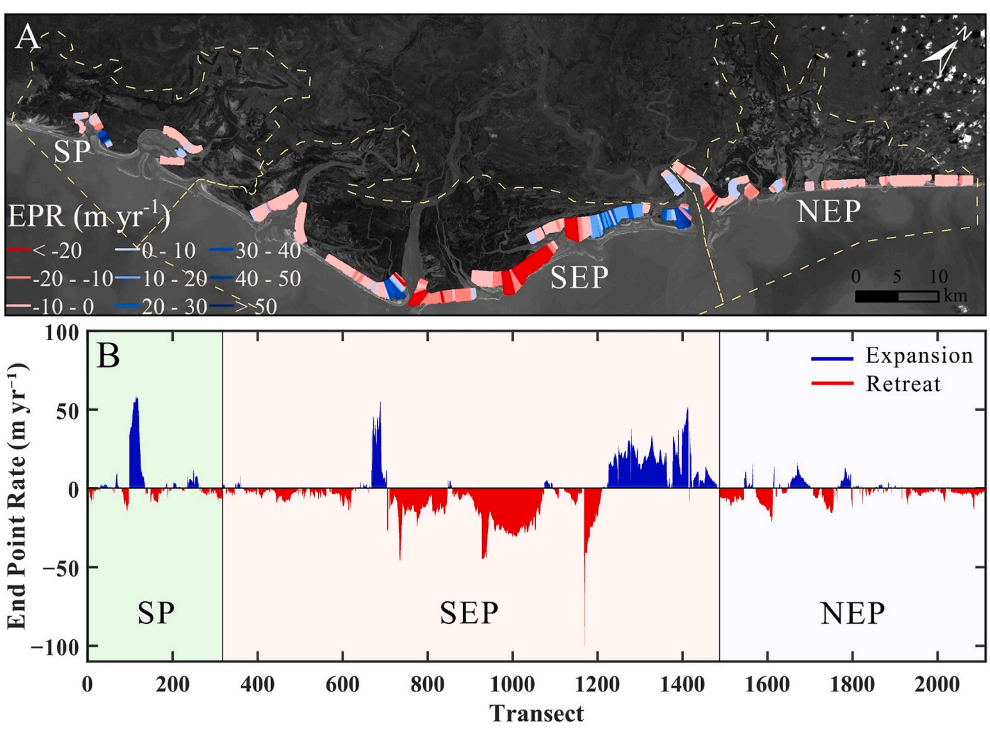

Fig. 5. Long-term shifts in the seaward mangrove edge of the Zambezi Delta (1989–2024).

(Table S6). Regionally, retreat remained dominant in the NEP and SEP at mean EPRs of -2.24 m yr^{-1} and -2.43 m yr^{-1}, respectively, where retreating, stable, and expanding transects accounted for 25.56%, 65.02%, and 9.42% in the NEP, and 38.12%, 39.66%, and 22.22% in the

SEP (Fig. 5; Table S6). In contrast, the SP recorded a mean EPR of 3.10 m yr^{-1} and showed a more mixed pattern, with 15.14% retreating, 67.19% stable, and 17.67% expanding, indicating slight expansion dominance under the conservative threshold (Fig. 5; Table S6). Although the conservative threshold inflated the proportion of stable coastline, retreat still exceeded expansion at the delta scale and within the NEP and SEP (Table S6).

3.3. Spatiotemporal dynamics of land cover transitions

Between 1989 and 2024, land cover in the Zambezi Delta underwent extensive transformation, driven by bidirectional exchanges among mangroves, terrestrial vegetation, bare land, and bare tidal flats. During the 1989–2003 period, mangrove gains significantly outpaced losses. Mangrove forests lost 4,260, 3,000, and 1110 ha to terrestrial vegetation, bare land, and bare tidal flats, respectively (Fig. 6A–C). These losses occurred primarily upstream of tidal channels in the SEP and SP and along the intertidal–terrestrial interface, while conversions to bare tidal flats were localized to the SEP and southwestern NEP coasts (Fig. 6A). Conversely, gross gains were higher, with mangroves replacing terrestrial vegetation (5930 ha), bare land (4200 ha), and bare tidal flats (2690 ha). These gains resulted from landward expansion across intertidal–terrestrial zones and seaward expansion along mudflats bordering NEP estuarine channels (Fig. 6A–C).

This dynamic reversed sharply between 2003 and 2024. Mangrove conversions to terrestrial vegetation (9830 ha), bare land (2260 ha), and bare tidal flats (2370 ha) far exceeded corresponding gains. This deficit drove the localized decline in mangrove area observed after 2001,

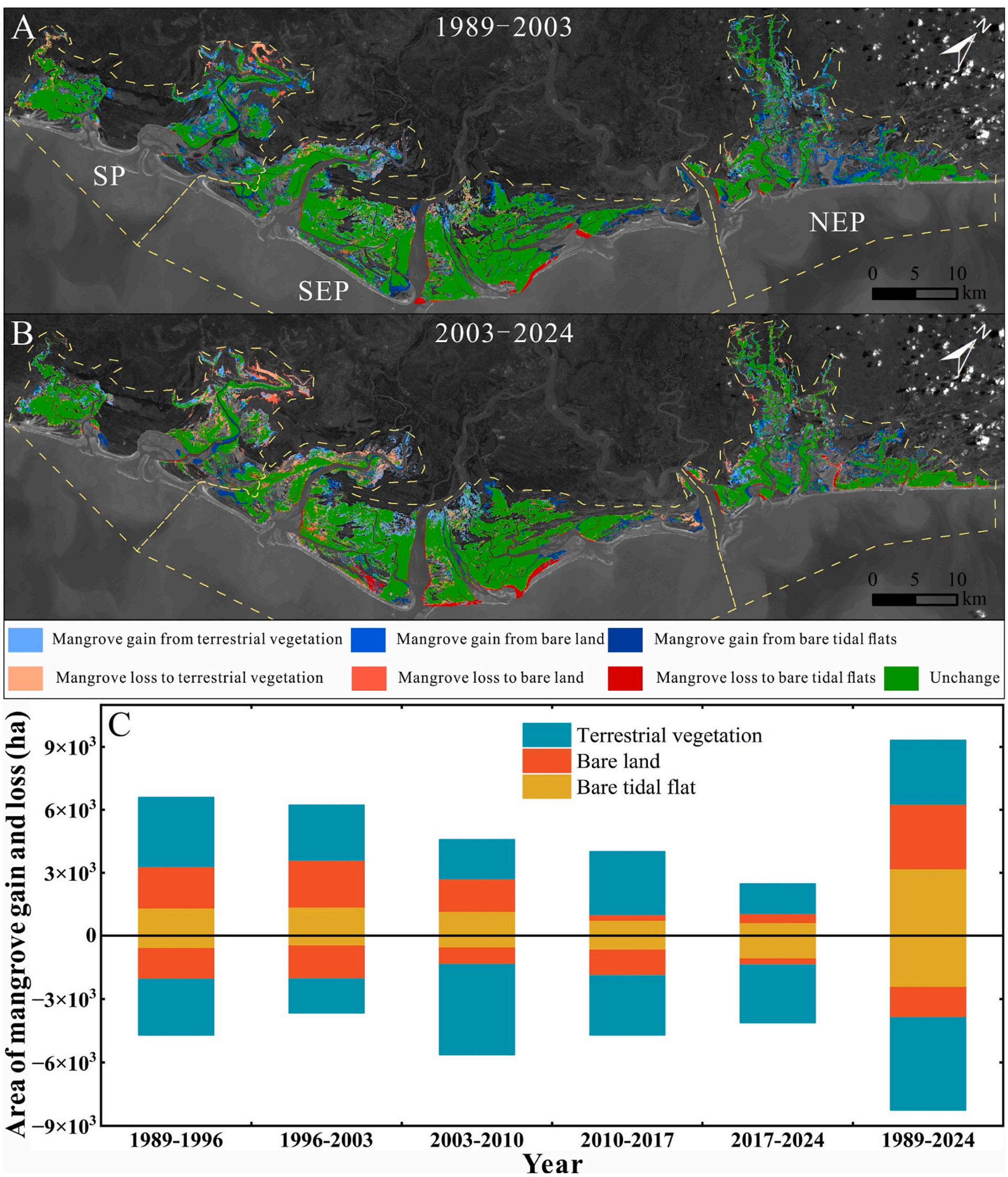

Fig. 6. Spatiotemporal dynamics of land cover in the Zambezi Delta (1989–2024). Land cover transitions during (A) 1989–2003 and (B) 2003–2024. (C) Conversions between mangroves and other land cover types for each period.

particularly across the SEP and SP (Fig. 2A and 6B–C). Losses to terrestrial vegetation and bare land were widespread upstream of tidal channels and in high-tide zones, whereas losses to bare tidal flats were concentrated along the SEP coast (Fig. 3C–E, 6B).

Cumulatively (1989–2024), gross mangrove gain (9320 ha) slightly outpaced gross loss (8260 ha), resulting in a net area increase (Fig. 2A and 6, S2). Delta-wide gains were evenly distributed among prior land covers: terrestrial vegetation (3050 ha), bare land (3070 ha), and bare tidal flats (3200 ha). In contrast, gross losses were heavily concentrated in the SEP and SP, driven predominantly by conversions to terrestrial vegetation (4370 ha) and bare tidal flats (2450 ha) (Fig. 6, S2).

3.4. Mangrove morphological responses to coastal hydrodynamics

Offshore wave climate was dominated by strong southeasterly waves across all three sub-regions, with the highest energy along the SEP, where 25.05% of waves exceeded 1 m in significant height and maxima reached 2–3 m (Fig. 7A–C, S3). Mangrove dynamics along the seaward edge displayed distinct responses to wave exposure. The most rapid retreat occurred in the SEP, the sub-region experiencing the highest wave energy, where the mangrove seaward edge retreat at a mean rate of -2.43 m yr^{-1} (Figs. 5 and 7B). Moreover, transects oriented directly into the prevailing southeasterly waves—where the mangrove edge faced the incoming wave direction—showed the greatest susceptibility to retreat (Fig. 7D–S4). By contrast, in wave-sheltered zones landward of sandbars and barrier islands, mangroves continued to expand (Fig. 5, S4).

Beyond wave forcing, seasonal residual currents flow northeastward along the Zambezi Delta coast during summer, autumn, and winter, reaching monthly mean velocities of up to 0.1 m s^{-1} (Fig. 8). These currents likely promote alongshore transport of sediment resuspended by southeasterly waves, with a portion delivered into tidal channels. Consistent with this, landward mangrove encroachment was widely observed within tidal channels of the SEP and NEP (Fig. 3, S2).

Concurrently, mangrove expansion within tidal channels was accompanied by progressive channel narrowing and localized mangrove degradation in the upstream reaches (Fig. 9A and B). Morphological measurements derived from remote sensing imagery along a representative 33-km tidal channel in the SP revealed a statistically significant narrowing trend. At Section a, located approximately 20 km from the upstream limit, the channel contracted at a mean rate of 6.79 m yr^{-1}. Further downstream at Section b, 28 km from the upstream limit, the narrowing rate nearly doubled, reaching 12.14 m yr^{-1} (Fig. 9C). This progressive channel infilling coincided with the transition of upstream mangroves into terrestrial vegetation (Fig. 9B).

4. Discussion

4.1. Hydrodynamic controls and the spatial heterogeneity of mangrove response

Mangrove colonization fundamentally requires bare, gently sloping

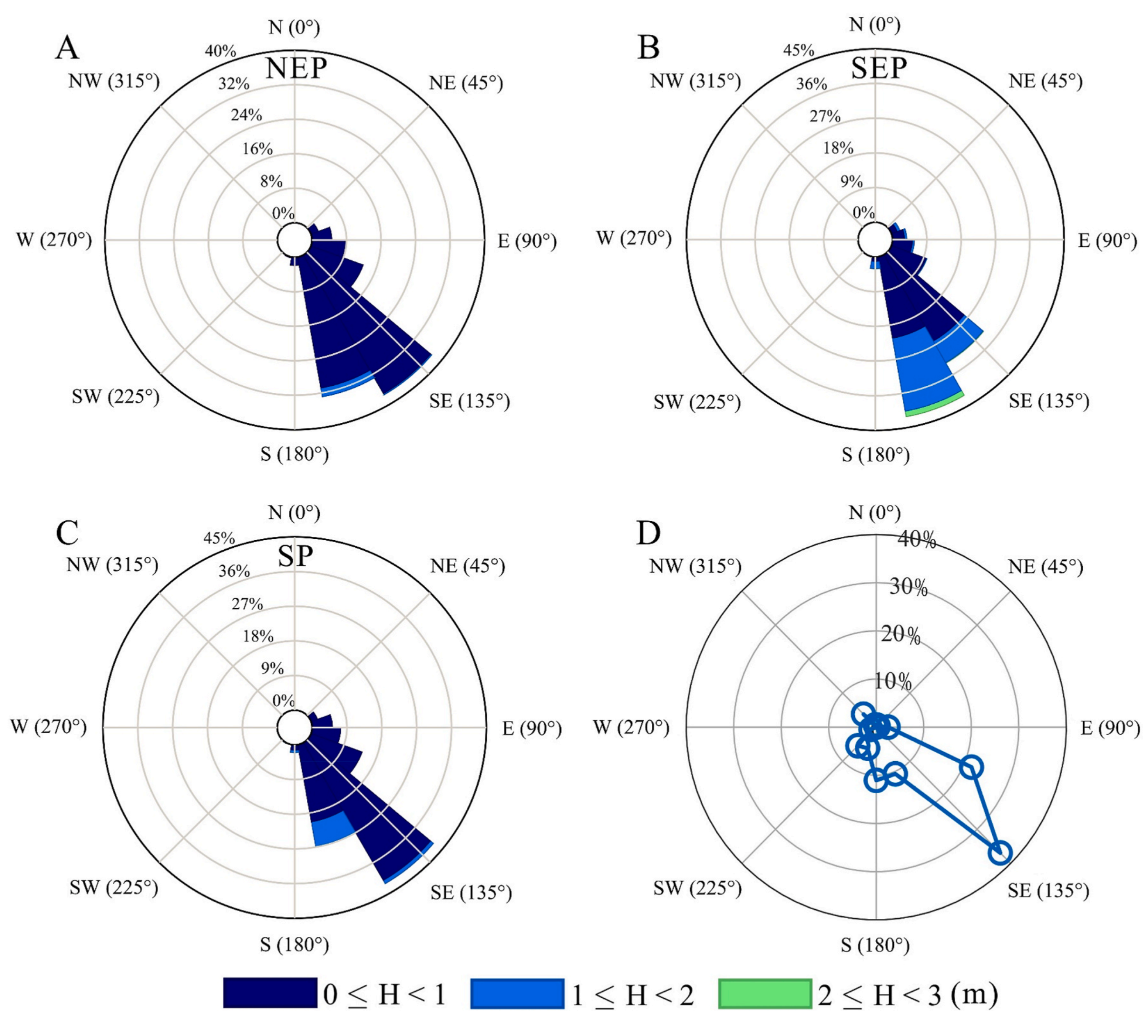

Fig. 7. Wave climate and seaward-edge retreat of mangroves in the Zambezi Delta. (A–C) Wave roses for the SP, SEP, and NEP, respectively. (D) Proportional distribution of transect orientations along the retreat seaward edge.

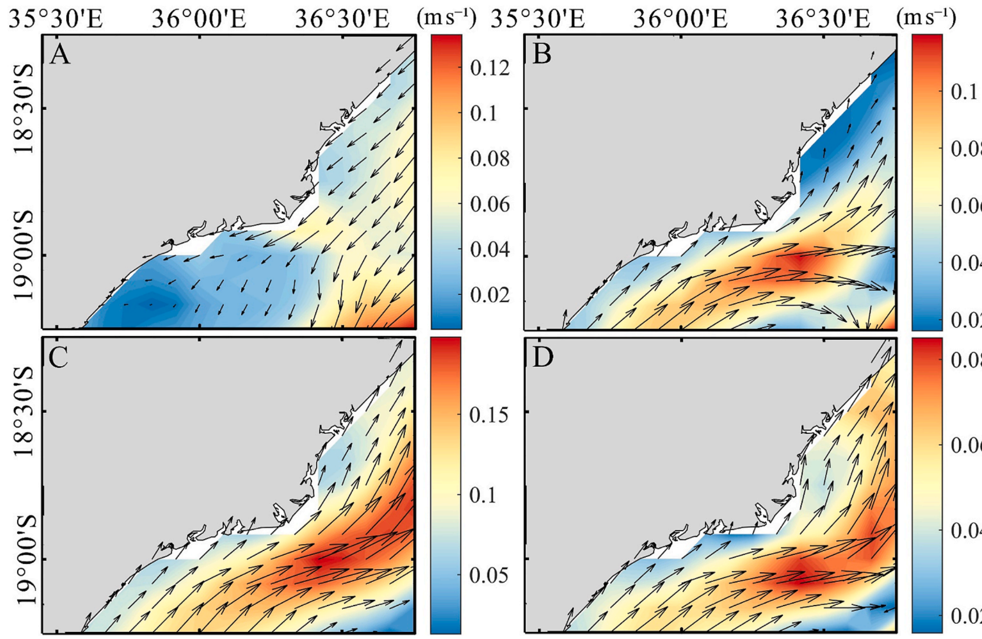

Fig. 8. Seasonal climatology of ocean currents in the Zambezi Delta during (A) spring, (B) summer, (C) autumn, and (D) winter.

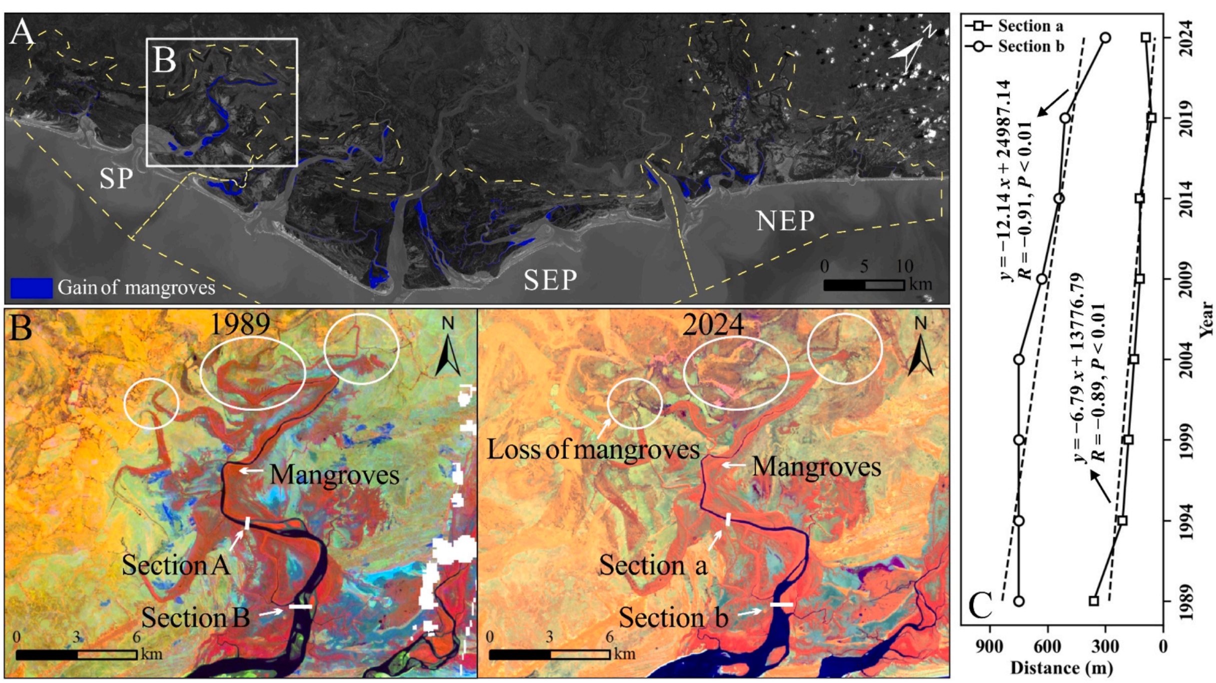

Fig. 9. Mangrove encroachment into tidal channels and associated upstream degradation in the Zambezi Delta. (A, B) In-channel mangrove expansion from 1989 to 2024. Upstream mangrove degradation in the SP is shown in (B), where two cross-sections (a and b) are marked. (C) Corresponding channel width variations at Sections a and b.

substrates provided by fluvial sediment deposition (Swales et al., 2019). In the Zambezi Delta, fluvial suspended sediment discharge exhibited an increasing trend from 1989 to 2020 (Fig. 1C); however, this trend must be interpreted within the longer-term context of upstream sediment regulation. The Kariba and Cahora Bassa dams, completed in 1959 and 1975 respectively, have substantially curtailed sediment delivery relative to pre-dam conditions by trapping coarse and fine fractions within their reservoirs (Ronco et al., 2010). Consequently, the increasing trend observed after 1989 does not signify a recovery toward natural sediment loads but rather reflects more recent sediment mobilization within the catchment, likely driven by accelerated land-use change, vegetation clearance, and soil disturbance. This interpretation aligns with Dethier et al. (2022), who reported that many rivers across the global hydrologic south have experienced rising suspended sediment fluxes in recent decades, particularly in basins subject to intensive deforestation and agricultural expansion.

Critically, this rising sediment supply did not produce a monotonic delta-wide mangrove expansion. Instead, mangrove area followed a two-phase trajectory of expansion (1989–2001) and subsequent contraction (Fig. 2A), with sharply divergent sub-regional outcomes.

This non-linearity demonstrates that sediment supply, while necessary, is insufficient on its own; its ecological consequences are mediated by local hydrodynamics that determine whether sediment is retained within mangrove-suitable environments or exported from them.

Two contrasting outcomes illustrate this mediation. Within sheltered tidal channels, attenuated tidal and fluvial energy promoted fine-sediment deposition, enabling 2653 ha of new mangrove establishment and channel narrowing rates of 6.79–12.14 m yr^{-1} (Fig. 9C). In contrast, along wave-exposed seaward margins—particularly the SEP, where 25.05% of waves exceeded 1 m in significant height (Fig. 7B)—wave-driven erosion overwhelmed sediment supply, producing a mean retreat of −2.43 m yr^{-1}. Transects facing the prevailing southeasterly waves were most vulnerable, while mangroves landward of sandbars and barrier islands continued to expand (Fig. 7D–S4). Analogous spatial mediation has been reported elsewhere: sediment-driven expansion in the Porong River Delta, and redistribution-dependent persistence in the Nanliu and Red River Deltas despite declining fluvial inputs (Beselly et al., 2021; Long et al., 2021, 2022).

4.2. Bio-geomorphic feedbacks and hydrological connectivity in tidal channels

Beyond seaward-edge dynamics, the bidirectional transitions between mangroves and terrestrial vegetation (Fig. 6) reveal an internally driven feedback mechanism that profoundly shapes mangrove distribution. Under regional sea-level rise of 3.0–3.5 mm yr^{-1} (Mikhailov and Mikhailova, 2010) and saline intrusion reaching 80 km inland (Beilfuss and Santos, 2001; Stringer et al., 2015), one would expect mangroves to advance landward at the expense of freshwater vegetation. This expectation is borne out during 1989–2003, when mangroves replaced 5930 ha of terrestrial vegetation in upstream zones.

Paradoxically, however, mangrove-to-terrestrial-vegetation conversions reached 9830 ha during 2003–2024, concentrated in high-tide and far-upstream zones. We propose that this reversal reflects a negative bio-geomorphic feedback mechanism intrinsic to mixed-energy deltas. Flow deceleration at the convergence of fluvial and tidal currents traps sediment within tidal channels; mangroves rapidly colonize the resulting mudflats, and their root systems amplify sediment retention (Bunting et al., 2022). The resulting progressive channel constriction (Fig. 9C) reduces the tidal prism and dampens upstream tidal propagation (Zhang et al., 2021), thereby isolating upper-estuary habitats from the saline inundation that sustains mangrove competitive dominance. Once tidal connectivity is lost, mangroves are progressively displaced by terrestrial vegetation or undergo desiccation.

This feedback mechanism reveals a critical dynamic regarding coastal wetland adaptation. Although external forcing such as sea-level rise initially promotes the inland migration of mangroves, internally generated geomorphic alterations—specifically, ongoing organic accretion and sediment trapping that reduce tidal prism and drive channel infilling, ultimately causing a seaward retreat of the tidal network (Van Maanen et al., 2015)—ultimately establish a strict spatial boundary on this advancement. Meanwhile, mangrove colonization progressively straightens and narrows tidal channels, fundamentally altering hydrodynamic gradients and accelerating the bio-geomorphic constriction of the network (Lee et al., 2022). Consequently, the progressive bio-geomorphic constriction of tidal networks functions as a largely unrecognized intrinsic limitation that restricts the long-term viability of mangrove ecosystems in the upper reaches of mixed-energy deltas. This feedback offers a mechanistic explanation for the spatially coherent pattern of upstream mangrove dieback observed across the SP and SEP (Figs. 4 and 9B), and underscores that mangrove evolution in mixed-energy deltas is driven by more than just external forcing—internally generated geomorphic feedbacks are similarly important.

4.3. Comparative perspectives across delta types and implications for management

With its relatively low population density, the Zambezi Delta experiences weaker direct anthropogenic pressure than the heavily populated Ganges, Irrawaddy, or Mekong Deltas, where mangrove degradation is largely human-driven (Phan and Stive, 2022; Shapiro et al., 2015; Xiong et al., 2024; Zhou et al., 2024). It therefore offers a valuable natural laboratory for isolating the hydrodynamic and bio-geomorphic controls on mangrove evolution.

The dynamics documented here highlight the distinctive character of mixed-energy deltas. Hydrodynamics in the Zambezi Delta play a dual role: southeasterly waves and alongshore currents erode exposed coastal margins, yet simultaneously redistribute resuspended sediment into sheltered tidal channels where it is trapped and stabilized by mangrove colonization. This differs from typical deltas—tide-dominated deltas (e.g., Nanliu) where tidal currents drive seaward mangrove expansion (Long et al., 2022); wave-dominated deltas where retreat predominates and expansion is confined to sheltered refugia (Long et al., 2025; Zhou et al., 2024); and river-dominated deltas where fluvial sediment sustains seaward progradation (Dai et al., 2024). Recognizing the Zambezi Delta as representative of a broader class of mixed-energy systems is essential for developing generalizable predictive frameworks of mangrove evolution.

These insights translate into three management priorities. First, along wave-exposed sectors of the NEP and SEP, engineering interventions such as bamboo fences or low-crested breakwaters can attenuate wave energy and stabilize retreating mangrove fronts (Akbar et al., 2017; Huang et al., 2023; Van Cuong et al., 2015). Second, the bio-geomorphic feedback identified here implies that in-channel mangrove expansion, though superficially beneficial, can ultimately undermine upstream mangrove persistence by severing tidal connectivity. Maintaining channel hydrological connectivity—through periodic dredging, targeted thinning of in-channel mangrove patches, or strategic channel management—should therefore be a primary objective, particularly as sea-level rise accelerates landward mangrove migration. Third, because increased fluvial sediment supply has not translated into consistent seaward expansion, basin-scale management must focus on sediment redistribution, not merely total input (Xiong et al., 2024; Zhou et al., 2024); estuarine sand mining and other activities that disrupt sediment pathways warrant strict regulation. The integration of remote sensing and machine learning into long-term monitoring frameworks provides a cost-effective foundation for the early warning and adaptive management systems needed to safeguard mangroves in the Zambezi Delta and analogous mixed-energy deltas worldwide.

4.4. Limitations

A primary limitation of this study is the ~31 km spatial resolution of the ERA5 reanalysis data. While adequate for characterizing offshore wave climatology, this resolution is insufficient to resolve complex nearshore processes, such as wave refraction, shoaling, and barrier island sheltering. Consequently, our analysis represents the offshore wave climate driving nearshore conditions, rather than a direct simulation of nearshore wave transformation. The sub-regional wave roses (Fig. 7, S3) thus reflect large-scale variations in offshore wave exposure across the 180-km coastline. Characterizing the localized nearshore wave climate would require subsequent downscaling using high-resolution numerical models.

Secondly, distinguishing mangroves from terrestrial vegetation relies partly on SWIR absorption associated with tidal inundation. Reduced tidal connectivity decreases canopy moisture, attenuating the SWIR signal. This may cause the classifier to register a transition to terrestrial vegetation prior to actual species turnover. Therefore, a fraction of the reported mangrove-to-terrestrial conversions may represent a spectral artifact rather than immediate ecological change. Nevertheless, this early spectral shift captures severe hydrological degradation, serving as a robust indicator of inevitable ecological succession toward terrestrial ecosystems.

Finally, suspended sediment estimates are derived from a global satellite-based dataset (Dethier et al., 2022). Uncertainty remains as to whether these values reflect purely fluvial discharge or include tidally resuspended sediments within the Zambezi Delta's ~80 km tidal reach. Given this ambiguity, we utilize the sediment record solely to identify broad temporal trends in sediment availability, avoiding direct quantitative correlations with mangrove area.

5. Conclusions

Using 35 years of Landsat imagery from 1989 to 2024 with fluvial sediment and hydrodynamic datasets, this study provides the first comprehensive assessment of mangrove spatiotemporal dynamics in the Zambezi Delta—a representative mixed-energy deltaic system. The main findings are as follows:

(1) Delta-wide mangrove area followed a two-phase trajectory, expanding from 1989 to 2001 at 307.08 ha yr^{-1}, before contracting through 2024 at −107.47 ha yr^{-1}. This overall pattern masked strong sub-regional divergence: the NEP experienced persistent net gain, the SEP shifted from expansion to decline after 2008, and the SP underwent sustained loss.

(2) Mangrove responses were controlled less by total fluvial sediment supply than by localized sediment redistribution. Despite an increasing trend in fluvial sediment discharge, mangroves did not exhibit sustained delta-wide expansion or consistent seaward progradation. Instead, strong southeasterly waves drove retreat along exposed seaward edges, especially in the NEP and SEP, whereas seasonal northeastward currents likely transported wave-resuspended sediment into sheltered tidal channels, promoting in-channel mangrove establishment and channel narrowing.

(3) Bio-geomorphic feedbacks played an important role in internal mangrove redistribution. Sedimentation and mangrove encroachment within tidal channels likely reduced channel width and weakened upstream tidal connectivity. This process may have limited saline inundation in upper-channel areas, contributing to localized mangrove degradation, dieback, and replacement by terrestrial vegetation.

CRediT authorship contribution statement

Tianliang Wu: Data curation, Formal analysis, Methodology, Writing – original draft. **Aoyang He:** Data curation, Methodology, Resources, Visualization, Writing – original draft. **Zhijun Dai:** Conceptualization, Data curation, Funding acquisition, Methodology, Project administration, Supervision, Writing – original draft, Writing – review & editing. **Yan Li:** Formal analysis, Methodology, Validation, Visualization. **Binyuan He:** Methodology, Resources, Visualization. **Qingxian Cao:** Validation, Visualization, Writing – review & editing. **Jinlan Lin:** Methodology, Validation, Writing – review & editing. **Xixing Liang:** Validation, Visualization, Writing – review & editing.

Declaration of competing interest

The authors declare that they have no known competing financial interests or personal relationships that could have appeared to influence the work reported in this paper.

Acknowledgements

This research was supported by the Shanghai International Science and Technology Cooperation Fund Project, China (23230713800; 23590780200; 24230740100).

Appendix A. Supplementary data

Supplementary data to this article can be found online at https://doi.org/10.1016/j.jenvman.2026.130111.

Data availability

Data will be made available on request.

References

Akbar, A.A., Sartohadi, J., Djohan, T.S., Ritohardoyo, S., 2017. The role of breakwaters on the rehabilitation of coastal and mangrove forests in West Kalimantan, Indonesia. Ocean Coast Manag. 138, 50–59.
Baloloy, A.B., Blanco, A.C., Ana, R.R.C.S., Nadaoka, K., 2020. Development and application of a new mangrove vegetation index (MVI) for rapid and accurate mangrove mapping. ISPRS J. Photogrammetry Remote Sens. 166, 95–117.
Barbier, E.B., Hacker, S.D., Kennedy, C., Koch, E.W., Stier, A.C., Silliman, B.R., 2011. The value of estuarine and coastal ecosystem services. Ecol. Monogr. 81 (2), 169–193.
Barbosa, F.M., Cuambe, C.C., Bandeira, S.O., 2001. Status and distribution of mangroves in Mozambique. South Afr. J. Bot. 67 (3), 393–398.
Beilfuss, R., Santos, D.D., 2001. Patterns of hydrological change in the Zambezi Delta, Mozambique. Program for the sustainable management of Cahora Bassa Dam and the Lower Zambezi Valley.
Bento, C.M., Beilfuss, R.D., Hockey, P.A., 2007. Distribution, structure and simulation modelling of the wattled crane population in the Marromeu Complex of the Zambezi Delta, Mozambique. Ostrich - J. Afr. Ornithol. 78 (2), 185–193.
Besselly, S.M., van der Wegen, M., Grueters, U., Reyns, J., Dijkstra, J., Roelvink, D., 2021. Eleven years of mangrove–Mudflat dynamics on the mud volcano-induced prograding delta in East Java, Indonesia: integrating UAV and satellite imagery. Remote Sens. 13 (6), 1084.
Besset, M., Gratiot, N., Anthony, E.J., Bouchette, F., Goichot, M., Marchesiello, P., 2019. Mangroves and shoreline erosion in the Mekong River delta, Viet Nam. Estuar. Coast Shelf Sci. 226, 106263.
Bhargava, R., Sarkar, D., Friess, D.A., 2021. A cloud computing-based approach to mapping mangrove erosion and progradation: case studies from the Sundarbans and French Guiana. Estuar. Coast Shelf Sci. 248, 106798.
Bryan-Brown, D.N., Connolly, R.M., Richards, D.R., Adame, F., Friess, D.A., Brown, C.J., 2020. Global trends in mangrove forest fragmentation. Sci. Rep. 10 (1), 7117.
Bunting, P., Rosenqvist, A., Hilarides, L., Lucas, R.M., Thomas, N., Tadono, T., Worthington, T.A., Spalding, M., Murray, N.J., Rebelo, L.M., 2022. Global mangrove extent change 1996–2020: global Mangrove Watch version 3.0. Remote Sens. 14 (15), 3657.
Dai, Z., Long, C., Mei, X., Fagherazzi, S., Xong, Y., 2024. Overestimation of mangroves deterioration from sea level rise in tropical deltas. Geophys. Res. Lett. 51 (19) e2024GL109675.
Dethier, E.N., Renshaw, C.E., Magilligan, F.J., 2022. Rapid changes to global river suspended sediment flux by humans. Science 376 (6600), 1447–1452.
Donato, D.C., Kauffman, J.B., Murdiyarso, D., Kurnianto, S., Stidham, M., Kanninen, M., 2011. Mangroves among the most carbon-rich forests in the tropics. Nat. Geosci. 4 (5), 293–297.
FAO, 2023. The World's Mangroves 2000–2020. Rome.
Gao, B.C., 1996. NDWI–A normalized difference water index for remote sensing of vegetation liquid water from space. Rem. Sens. Environ. 58 (3), 257–266.
Hasim, H., 2021. Mangrove ecosystem, seagrass, coral reef: its role in self-purification and carrying capacity in coastal areas. International Journal Papier Advance and Scientific Review 2 (1), 37–49.
Hersbach, H., Bell, B., Berrisford, P., Biavati, G., Horányi, A., Muñoz Sabater, J., Nicolas, J., Peubey, C., Radu, R., Rozum, I., Schepers, D., Simmons, A., Soci, C., Dee, D., Thépaut, J.-N., 2023. ERA5 hourly data on single levels from 1940 to present. Copernicus Climate Change Service (C3S) Climate Data Store (CDS). https://doi.org/10.24381/cds.adbb2d47.
Huang, Z., Dai, Z., Wang, R., Zhou, X., Pang, W., Luo, J., Feng, B., Hu, B., 2023. Dramatical hydro-sedimentary changes induced by bamboo fences over mangrove tidal flat of the largest delta in Beibu Gulf, southwestern China. Acta Oceanol. Sin. 42 (7), 103–115.
Huete, A., Didan, K., Miura, T., Rodriguez, E.P., Gao, X., Ferreira, L.G., 2002. Overview of the radiometric and biophysical performance of the MODIS vegetation indices. Rem. Sens. Environ. 83 (1–2), 195–213.
Jia, M., Wang, Z., Mao, D., Ren, C., Song, K., Zhao, C., Wang, C., Xiao, X., Wang, Y., 2023. Mapping global distribution of mangrove forests at 10-m resolution. Science Bulletin 68 (12), 1306–1316.
Lee, K.Y., Shih, S., Huang, Z.Z., 2022. Mangrove colonization on tidal flats causes straightened tidal channels and consequent changes in the hydrodynamic gradient and siltation potential. J. Environ. Manag. 314, 115058.
Lellouche, J.M., Greiner, E., Bourdallé-Badie, R., Garric, G., Melet, A., Drévillon, M., Bricaud, C., Hamon, M., Le Galloudec, O., Regnier, C., Candela, T., Testut, C.-E., Gasparin, F., Ruggiero, G., Benkiran, M., Drillet, Y., Le Traon, P.-Y., 2021. The

copernicus Global 1/12° Oceanic and Sea ice GLORYS12 reanalysis. Front. Earth Sci. 9, 698876.
Long, C., Dai, Z., Mei, X., Liang, X., Zhang, X., Xi, Y., Wang, R., Binh, N.A., Van, C.M., Cheng, J., 2025. Machine learning-based detection of dynamic changes in mangrove forest, Beilun Estuary. Ocean Coast Manag. 266, 107696.
Long, C., Dai, Z., Wang, R., Lou, Y., Zhou, X., Li, S., Nie, Y., 2022. Dynamic changes in mangroves of the largest delta in northern Beibu Gulf, China: reasons and causes. For. Ecol. Manag. 504, 119855.
Long, C., Dai, Z., Zhou, X., Mei, X., Van, C.M., 2021. Mapping mangrove forests in the red river delta, Vietnam. For. Ecol. Manag. 483, 118910.
Lymburner, L., Bunting, P., Lucas, R., Scarth, P., Alam, I., Phillips, C., Ticehurst, C., Held, A., 2020. Mapping the multi-decadal mangrove dynamics of the Australian coastline. Rem. Sens. Environ. 238, 111185.
Mazzaretto, O.M., Menendez, M., 2024. A worldwide coastal analysis of the climate wave systems. Front. Mar. Sci. 11, 1385285.
McFeeters, S.K., 1996. The use of the Normalized Difference Water Index (NDWI) in the delineation of open water features. Int. J. Rem. Sens. 17 (7), 1425–1432.
Menéndez, P., Losada, I.J., Torres-Ortega, S., Narayan, S., Beck, M.W., 2020. The global flood protection benefits of mangroves. Sci. Rep. 10 (1), 4404.
Mikhailov, V.N., Kravtsova, V.I., Isupova, M.V., 2015. Impact of reservoirs on the hydrological regime and morphology of the lower reaches and delta of the Zambezi River (Mozambique). Water Resour. 42 (2), 170–185.
Mikhailov, V.N., Mikhailova, M.V., 2010. Regularities in sea level rise impact on the hydrological regime and morphological structure of river deltas. Water Resour. 37 (1), 1–15.
Murdiyarso, D., Purbopuspito, J., Kauffman, J.B., Warren, M.W., Sasmito, S.D., Donato, D.C., Manuri, S., Krisnawati, H., Taberima, S., Kurnianto, S., 2015. The potential of Indonesian mangrove forests for global climate change mitigation. Nat. Clim. Change 5 (12), 1089–1092.
Phan, M.H., Stive, M.J., 2022. Managing mangroves and coastal land cover in the Mekong Delta. Ocean Coast Manag. 219, 106013.
Rogers, K.G., Goodbred Jr, S.L., 2014. The Sundarbans and Bengal Delta: the world's largest tidal mangrove and delta system. In: Landscapes and Landforms of India. Springer Netherlands, Dordrecht, pp. 181–187.
Ronco, P., Fasolato, G., Nones, M., Di Silvio, G., 2010. Morphological effects of damming on lower Zambezi River. Geomorphology 115, 43–55.
Rouse, J.W., Haas, R.H., Schell, J.A., Deering, D.W., 1974. Monitoring vegetation systems in the Great Plains with ERTS. In: Proceeding of Erts-1 Symposium.
Sasmito, S.D., Basyuni, M., Kridalaksana, A., Saragi-Sasmito, M.F., Lovelock, C.E., Murdiyarso, D., 2023. Challenges and opportunities for achieving Sustainable Development Goals through restoration of Indonesia's mangroves. Nat. Ecol. Evol. 7 (1), 62–70.
Shapiro, A.C., Trettin, C.C., Küchly, H., Alavinapanah, S., Bandeira, S., 2015. The mangroves of the Zambezi Delta: increase in extent observed via satellite from 1994 to 2013. Remote Sens. 7 (12), 16504–16518.
Sreelakshmi, S., Bhaskaran, P.K., 2020. Wind-generated wave climate variability in the Indian Ocean using ERA-5 dataset. Ocean. Eng. 209, 107486.
Stringer, C.E., Trettin, C.C., Zarnoch, S.J., Tang, W., 2015. Carbon stocks of mangroves within the Zambezi River Delta, Mozambique. For. Ecol. Manag. 354, 139–148.
Swales, A., Reeve, G., Cahoon, D.R., Lovelock, C.E., 2019. Landscape evolution of a fluvial sediment-rich Avicennia marina mangrove forest: insights from seasonal and inter-annual surface-elevation dynamics. Ecosystems 22 (6), 1232–1255.
Thieler, E.R., Himmelstoss, E.A., Zichichi, J.L., Ergul, A., 2009. The Digital Shoreline Analysis System (DSAS) version 4.0–an ArcGIS extension for calculating shoreline change (No. 2008–1278). US Geological Survey.
Trettin, C.C., Stringer, C.E., Zarnoch, S.J., 2016. Composition, biomass and structure of mangroves within the Zambezi River Delta. Wetl. Ecol. Manag. 24, 173–186.
Tweddle, D., Cowx, I.G., Peel, R.A., Weyl, O.L.F., 2015. Challenges in fisheries management in the Zambezi, one of the great rivers of Africa. Fish. Manag. Ecol. 22, 99–111.
Van Cuong, C., Brown, S., To, H.H., Hockings, M., 2015. Using Melaleuca fences as soft coastal engineering for mangrove restoration in Kien Giang, Vietnam. Ecol. Eng. 81, 256–265.
Van Maanen, B., Coco, G., Bryan, K.R., 2015. On the ecogeomorphological feedbacks that control tidal channel network evolution in a sandy mangrove setting. Proc. R. Soc. A 471 (2180), 20150115.
Wang, Z., Liu, K., Cao, J., Peng, L., Wen, X., 2022. Annual change analysis of mangrove forests in China during 1986–2021 based on Google Earth Engine. Forests 13 (9), 1489.
Worthington, T.A., Zu Ermgassen, P.S., Friess, D.A., Krauss, K.W., Lovelock, C.E., Thorley, J., Tingey, R., Woodroffe, C.D., Bunting, P., Cormier, N., Lagomasino, D., Lucas, R., Murray, N.J., Sutherland, W.J., Spalding, M., 2020. A global biophysical typology of mangroves and its relevance for ecosystem structure and deforestation. Sci. Rep. 10 (1), 14652.
Wu, R., Dai, Z., Mei, X., Luo, J., Fagherazzi, S., 2025a. Profiling of mangrove forest dynamics in the Fly River delta, Papua New Guinea. Mar. Pollut. Bull. 217, 118119.
Wu, T., Pang, W., Wang, R., Huang, H., Shen, S., Huang, C., Hu, B., 2025b. Detecting dynamic changes in mangrove forests in the Dandou Sea, Beibu Gulf. Front. Earth Sci. 1–19.
Xiong, Y., Dai, Z., Long, C., Liang, X., Lou, Y., Mei, X., Nguyen, B.A., Cheng, J., 2024. Machine Learning-Based examination of recent mangrove forest changes in the western Irrawaddy River Delta, Southeast Asia. Catena 234, 107601.
Xu, H., 2006. Modification of normalised difference water index (NDWI) to enhance open water features in remotely sensed imagery. Int. J. Rem. Sens. 27 (14), 3025–3033.
Yang, G., Huang, K., Sun, W., Meng, X., Mao, D., Ge, Y., 2022. Enhanced mangrove vegetation index based on hyperspectral images for mapping mangrove. ISPRS J. Photogrammetry Remote Sens. 189, 236–254.
Zhang, P., Yang, Q., Wang, H., Cai, H., Liu, F., Zhao, T., Jia, L., 2021. Stepwise alterations in tidal hydrodynamics in a highly human-modified estuary: the roles of channel deepening and narrowing. J. Hydrol. 597, 126153.
Zhou, X., Dai, Z., Pang, W., Wang, J., Long, C., 2022. Wave attenuation over mangroves in the Nanliu Delta, China. Front. Mar. Sci. 9, 874818.
Zhou, Y., Dai, Z., Liang, X., Cheng, J., 2024. Machine learning-based monitoring of mangrove ecosystem dynamics in the Indus Delta. For. Ecol. Manag. 571, 122231.